4-1-2006

The High-Resolution Structures of the Neutral and the Low pH Crystals of Aminopeptidase from *Aeromonas proteolytica*

William Desmarais
Brandeis University

David L. Bienvenue
Utah State University

Krzysztof P. Bzymek
Utah State University

Gregory A. Petsko
Brandeis University

Dagmar Ringe
Brandeis University

See next page for additional authors

Accepted version. *Journal of Biological Inorganic Chemistry*, Vol. 11, No. 4 (April 2006): 398-408. DOI.
Richard Holz was affiliated with the Utah State University at the time of publication.

JBIC Journal of Biological Inorganic Chemistry, Vol. 11, No. 4 (June 2006): 398-408. DOI.

The high-resolution structures of the neutral and the low pH crystals of aminopeptidase from *Aeromonas proteolytica*

William Desmarais
Program in Biophysics and Structural Biology, Brandeis University, Waltham
The Rosenstiel Basic Medical Sciences Research Center, MS029Brandeis University, Waltham

David L. Bienvenue
Department of Chemistry and Biochemistry, Utah State University, Logan

Krzysztof P. Bzymek
Department of Chemistry and Biochemistry, Utah State University, Logan

Gregory A. Petsko
The Rosenstiel Basic Medical Sciences Research Center, MS029Brandeis University, Waltham
Department of Chemistry, Brandeis University, Waltham
Department of Biochemistry, Brandeis University, Waltham

Dagmar Ringe
The Rosenstiel Basic Medical Sciences Research Center, MS029Brandeis University, Waltham
Department of Chemistry, Brandeis University, Waltham
Department of Biochemistry, Brandeis University, Waltham

Richard C. Holz
Department of Chemistry, Marquette University, Milwaukee, WI
Department of Chemistry and Biochemistry, Utah State University, Logan

Abstract

The aminopeptidase from *Aeromonas proteolytica* (AAP) contains two zinc ions in the active site and catalyzes the degradation of peptides. Herein we report the crystal structures of AAP at 0.95-Å resolution at neutral pH and at 1.24-Å resolution at low pH. The combination of these structures allowed the precise modeling of atomic positions, the identification of the metal bridging oxygen species, and insight into the physical properties of the metal ions. On the basis of these structures, a new putative catalytic mechanism is proposed for AAP that is likely relevant to all binuclear metalloproteases.

Keywords

Crystallization, Electronic structure

Abbreviations

AAP	Aminopeptidase from *Aeromonas proteolytica*
BuBA	1-Butaneboronic acid
CSD	Cambridge Structural Database
ESD	Estimated standard deviation
HEPES	4-(2-Hydroxyethyl)-1-piperazineethanesulfonic acid
LPA	l-Leucinephosphonic acid
rms	Root mean square
Tris	Tris(hydroxymethyl)aminomethane

The coordinates for the 0.95-Å resolution structure and the 1.24-Å structure at pH 4.7 were deposited in the RCSB Protein Data Bank and have PDB ID numbers of 1RTQ and 2DEA, respectively.

Introduction

Bridged bimetallic (binuclear) enzymes contain two metal ions held in close proximity by a protein ligand and/or an oxygen atom, usually from bulk solvent, that spans two metal ions. These enzymes catalyze diverse reactions that include but are not limited to hydrolysis, isomerization, dehydration, and redox chemistry [1, 2, 3, 4]. They utilize most first-row transition metal ions and can be either homonuclear or heteronuclear. The physical properties of the two metal ions determine their Lewis acidities and, in turn, regulate the activity of the enzymes. Although the exact role of each metal ion during a given reaction cycle is not completely understood, it has been proposed that both metal ions are necessary to recognize and bind substrate, to activate the attacking nucleophile, and to stabilize intermediates of the reaction.

As a model system for bridged bimetallic enzymes, we have studied the extracellular, broad-specificity aminopeptidase from *Aeromonas proteolytica* (AAP). AAP is a 30-kDa, monomeric enzyme that utilizes two zinc(II) ions in its active site to remove N-terminal amino acids from peptides or proteins [5]. A chemical reaction mechanism has been proposed for AAP [6] in which the substrate binds to AAP by first coordinating the carbonyl oxygen of the N-terminal amino acid to Zn_1 followed by the coordination of the N-terminal amine to Zn_2. An activated water molecule then attacks the scissile bond at the carbonyl carbon, resulting in the formation of a gem diolate that is stabilized by interactions with both zinc ions. A conserved active-site residue, Glu_{151}, accepts

a proton from the bridging water molecule and then transfers it to the penultimate amino nitrogen of the new N terminus [7]. Finally, the enzyme returns to its native state upon the release of products and the addition of a new bridging water species. In this mechanism, the role of Zn_1 is to activate the nucleophilic water molecule from H_2O to OH^-, to activate the carbonyl carbon of the substrate, and to position the nucleophile for attack on the substrate. The role of Zn_2 is to assist in lowering the pK_a of the bridging water molecule, to provide enhanced specificity for and to orient N-terminal peptide substrates, and to stabilize intermediates in the reaction pathway.

Although structural and spectroscopic studies have provided a great deal of evidence for the role of each metal ion during the catalytic reaction cycle of AAP, many questions remain unanswered: Why are two metal ions employed in this and most other aminopeptidases? What is the protonation state of the bridging solvent molecule in the resting enzyme? When does the bridging solvent become activated to a nucleophile? What changes in the enzyme are required to accommodate substrate binding and the various intermediate states? To completely understand the role of each metal ion in AAP with respect to the catalytic reaction cycle, it is essential to know the precise position of every atom in the active site, including those of the hydrogen atoms. Two very important hydrogen atoms are those attached to the bridging oxygen. For AAP to perform the hydrolysis step, the bridging water presumably must be activated from H_2O to OH^-. As a first step in the determination of the protonation states of the metal ligands, the bridging oxygen, and Glu_{151} in AAP, we have determined the 1.20-Å resolution structure of native AAP at pH 8.0 in a tris(hydroxymethyl)aminomethane (Tris) buffer [8]. This structure showed a single molecule of Tris chelated to the two metal ions in the active site, making it impossible to identify the protonation state of the bridging oxygen and the active-site amino acids. Subsequently, we removed any interference caused by Tris by crystallizing the protein in 4-(2-hydroxyethyl)-1-piperazineethanesulfonic acid (HEPES) buffer.

Here we present the 0.95-Å resolution structure of AAP in HEPES buffer, pH 7.5, and the 1.24-Å resolution structure of AAP at pH 4.5 in acetate buffer. These high-resolution structures have led to a very precise analysis of AAP's active site, determination of the identity of the protonation state of the bridging oxygen, based on bonding distances, assignment of the double-bond distribution for the active-site carboxylates, and observation of a change in the coordination number of the proposed catalytic zinc ion at low pH, which may serve as a model for the first step in the reaction pathway. In the absence of electron density corresponding to hydrogen atoms, precise coordination distances can be used to establish the identity of the bridging water species by comparing its Zn–O bond distances. A survey of the Cambridge Structural Database (CSD) [9] and ab initio calculations [10] have provided Zn–OH and $Zn–OH_2$ bonding distances that should serve as standards for comparing the precise bonding distances obtained in protein crystal structures determined at ultrahigh resolutions. The increased quality of the electron density maps at 0.95-Å resolution has also allowed for a more detailed view of some hydrogen positions, the solvent region, and electron distribution in the active-site than was possible at 1.20-Å resolution.

Materials and methods

Enzyme purification

All chemicals used in this study were purchased commercially and were of the highest quality available. AAP was purified from a stock culture kindly provided by Céline Schalk. Cultures were grown according to the previously reported protocol with minor modifications [6] to the growth media. Purified enzyme was stored at −196 °C until needed.

Spectrophotometric assay

AAP activity was measured by monitoring the hydrolysis of 0.5 mM l-leucine *p*-nitroanilide [10 mM *N*-tris(hydroxymethyl)methylglycine, pH 8.0] spectrophotometrically at 25 °C by monitoring the formation of *p*-nitroaniline [6]. The extent of hydrolysis was calculated by monitoring the increase in absorbance at 405 nm ($\Delta\varepsilon$

$_{405}$ value of *p*-nitroaniline of 10,800 M^{-1} cm^{-1}). One unit is defined as the amount of enzyme that releases 1 µmol *p*-nitroaniline at 25 °C in 60 s. Depletion of enzyme-bound zinc or cobalt was prevented by the addition of 0.1 mM $ZnSO_4$ or $CoCl_2$ to the buffer. The specific activity of purified Zn(II)-bound AAP was typically found to be 120 U mg^{-1} of enzyme. Enzyme concentrations were determined from the absorbance at 280 nm with the value ε_{280}=41,800 M^{-1} cm^{-1} [6].

Crystallization

For crystallization, the buffer was exchanged by washing three times and concentrating to 16 mg ml^{-1} in 10 mM HEPES, pH 7.5, 10 mM KSCN, and 0.4 M NaCl, using a Microcon-10 filtration system. The protein was crystallized using the conditions reported previously [11] with the exception that Tris was replaced with HEPES [12]. Crystals with dimensions 0.5×0.5×0.3 mm^3 were obtained in 48 h and were shown to be isomorphous with the native crystals that were crystallized in a Tris buffer.

Data collection and processing

All diffraction data were collected at the Advanced Photon Source/BioCARS 14 BM-C station with a wavelength of 1.00 Å, a size of 0.150×0.250 mm^2, and operation at 90–60 mA as noted [8]. An AAP crystal was removed from the hanging drop, soaked in mother liquor containing 10% glycerol for 1 min, coated with Paratone-N oil, mounted in a 0.5-mm Hampton Research CryoLoop, and flash-cooled to −173 °C in liquid nitrogen. Data were collected in two steps using a single crystal beginning at the same orientation. First, high-resolution data were obtained by exposing the crystal to X-rays for 5 s per frame. Because of the low mosaicity of the crystal (estimated to be 0.25° by calculating the width of two reflections at half of their peak heights), the crystal was rotated about its omega axis in 0.3° increments for a total of 100°. The crystal-to-detector distance was 150 mm with a detector 2ϑ angle of 30°. Second, the low-resolution data were collected by reducing the exposure time to 0.5 s, moving the 2ϑ angle to 0°, and increasing the sample-to-detector distance to 200 mm. For this experiment, a helium cone was placed between the sample and the detector to reduce the absorption of X-rays by air. To observe the changes at low pH, a second crystal was removed from its hanging drop and soaked three times in 100 mM sodium acetate, pH 4.5, 100 mM KSCN, and 4.5 M NaCl for 30 min. The crystal was flashed-cooled as described earlier and data were collected as described for the low-resolution data collection. Because the detector distance was 100 mm, a helium cone was not used. The crystal was exposed for 10 s per frame and rotated about its phi axis in 0.5° increments.

The data were processed and scaled using Denzo and Scalepack, respectively [13]. For the AAP crystal at pH 7.5, the high- and low-resolution data collections showed little or no radiation damage relative to the first image. The scale factor for the final image of the high-resolution data set was 0.72, while that for the low-resolution data set was 1.32. The data from both sets were merged as described in the Scalepack manual. The scale factors for the AAP crystal at pH 4.5 also did not show much radiation damage with a final image scale factor of 0.92.

Both crystals were isomorphous with that of the published native structure and the phases from the published native structure (PDB ID 1AMP) [12] were used to generate the starting model. The two zinc ions and water molecules were excluded from the original coordinate file. Refinement for both data sets was carried out using the software package CNS [14] followed by SHELX. An R_{free} data set was made using 10% of the total unique reflections [14]. The refinement program, CNS, was used for a rigid-body refinement using reflections from 30.0- to 4.0-Å resolution range and for several rounds of isotropic positional refinement using incrementally higher resolution data to 1.20 Å (1.24 Å for the low pH structure). The two zinc ions were added after the first positional refinement and water molecules were added after each round of positional refinement. The final CNS model was then refined in SHELX-97 using the procedure outlined on page 8-8 of the manual [15]. In this procedure, diffuse solvent was refined, followed by anisotropic refinement of the thermal parameters for all atoms, resulting in approximately a 3% drop in the R_{factor} and R_{free} of each structure.

For the 0.95-Å resolution structure, all of the data to 0.95-Å resolution were added after anisotropic refinement of the thermal parameters, followed by the addition of hydrogen atoms to the atomic model. The addition of hydrogen atoms does not add any variable parameters to the refinement, as their positions are fixed by the geometry of the X–H bonds. The structure was refined almost to convergence. To obtain geometric estimated standard deviations (ESDs) on all geometric parameters, a blocked-matrix least-squares refinement was performed. For this stage of refinement, the protein was reduced into blocks of 32 amino acids which were refined in different cycles. The blocks contained overlapping residues so that every ESD could be estimated with all contributing atoms being refined in at least one of the refinement cycles. Also, in the blocked least-squares method, the anisotropic displacement parameters are held fixed, reducing the number of parameters by 3. After each round of refinement with SHELX-97, ARP/warp [16] was used to add water molecules. As a final step, all the data were combined. The final data processing and refinement statistics are outlined in Table 1.

Table 1. Data processing and refinement statistics for the structures of native aminopeptidase from *Aeromonas proteolytica* at 0.95-Å resolution and at pH 4.5

Crystal data		
Resolution (Å)	0.95	1.24
pH	7.5	4.5
Space group	$P6_122$	$P6_122$
Unit cell parameters (Å)	$a=b=109.94$, $c=91.34$	$a=b=109.94$, $c=91.34$
Data processing		
No. of observed reflections	3,348,266	1,877,810
No. of unique reflections	191,127	81,189
R_{merge}, overall (%)	6.4	7.4
Completeness, overall (%)	95	95.6
Highest-resolution shell (Å)	0.98–0.95	1.29–1.24
Completeness, outer shell (%)	59	65
R_{merge}, outer shell (%)	23	34.6
$\langle I \rangle / \langle \sigma_I \rangle$, outer shell	2.5	2.3
Model refinement		
Resolution range (Å)	27–0.95	30–1.24
R_{factor} (%)	13.5	15.3
R_{free} (%)	15.1	16.3
No. of protein atoms	2,400	2,400
No. of metal ions	5	3
No. of SCN^-	2	0
No. of water molecules	322	393
No. of potential hydrogen atoms	238	Not analyzed
B-factor model	Anisotropic	Isotropic
Root-mean-square deviation from ideality		
Bond lengths (Å)	0.02	0.02
Angle distances (Å)	0.03	0.03

Identification of possible hydrogen positions was performed as previously described [8]. The 900 peaks found by SHELXL were then analyzed by comparing the position of the peak on a $F_{obs}-F_{calc}$ electron density map calculated without the presence of hydrogen atoms with that of the calculated hydrogen position and by measuring the distance between the center of the peak and the associated protein atom. The final R_{factor} of the structure is 13.5% with an R_{free} of 15.3% using all measured data. Since the atomic restraints were released, ESDs for each bond distance could be calculated. For the pH 4.5 structure solved at 1.25-Å resolution, the final R_{factor} is 15.1% with an R_{free} of 16.3%.

Results and discussion

A model of AAP at 0.95-Å resolution

The reaction mechanism step at which deprotonation of the bridging solvent molecule occurs, the most likely candidate to function as the nucleophile, is unknown. For the bridging solvent molecule to be a good nucleophile, it must be activated from H_2O to OH^- and, it is believed, become terminally coordinated to only one of the metal ions early in the reaction pathway. We used atomic-resolution X-ray crystallography in an attempt to identify the protonation states of the active-site amino acids and the bridging oxygen in the native enzyme. The high-resolution structure of native AAP (1.20-Å resolution) in Tris buffer revealed a molecule of Tris coordinated to both metal ions. Although this structure did not provide any insight into the locations of the active-site hydrogen atoms, it did suggest that Zn_2 does not play a major role in substrate recognition. Subsequently, Tris buffer was replaced by HEPES buffer during crystallization and herein we present the crystal structure of native AAP to 0.95-Å resolution.

The 0.95-Å resolution structure of AAP overlaid with the 1.20-Å resolution structure with a root-mean-square (rms) deviation of 0.30 Å for the 291 structurally equivalent C_α atoms, indicating there were no major conformational changes between the two structures. These data now allow the visualization of all but two of the protein residues, which are located in flexible loop regions, in an electron density map with coefficients $2F_{obs}-F_{calc}$ contoured at the level of 1.5σ (Fig. 1). Increased definition in the electron density of the bound solvent regions allowed for the detection of bound small molecules that could not be previously assigned at 1.20-Å resolution. On the surface of the protein we identified three monovalent metal ions that coordinate at least one protein amino acid residue and link a second protein molecule through water networks as well as two thiocyanate ions, which are components of the crystallization buffer. The final model of our structure at 0.95-Å resolution consists of 291 amino acids, 322 water molecules including the bridging water species, three sodium ions, and two SCN^-.

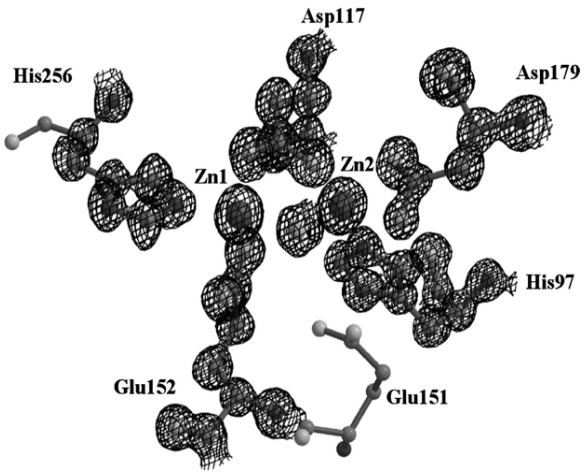

Fig. 1. $2F_o-F_c$ electron density map corresponding to the active-site amino acids contoured at 1.5σ. Electron density for Glu_{151} is not shown for clarity

Hydrogen atom location

At 1.20-Å resolution it was possible to locate the positions of some hydrogen atoms by directly observing their electron density on a Fourier difference electron density map with coefficients $F_{obs}-F_{calc}$ (Table 2) [8]. Of the 135 electron density peaks assigned as potential hydrogen atoms, they were all located within 0.3 Å of the ideal hydrogen covalent bonding distance of about 1.0 Å for N–H, C–H, and O–H. All 135 peaks had electron density levels higher than 1.5σ (0.16e^- Å^{-3}). A total of 108 peaks corresponded to carbon hydrogen atoms, with 40 of those belonging to C_α and 68 to side chain carbons. The remaining 25 peaks correspond to amide nitrogen hydrogen atoms. Two additional peaks were found in positions that are typical for hydrogen bonds. All of these peaks were found in well-ordered parts of the protein.

Table 2. The number of peaks in Fourier difference maps with coefficients $F_{obs}-F_{calc}$ at 0.95- and 1.20-Å resolutions and the associated atom types

Number of hydrogen atoms (0.95 Å)	Atom type	Number of hydrogen atoms (1.20 Å)
48	Main chain C	40
136	Side chain C	68
45	Main chain N	25
8	Side chain N	0

Because of the precision in the atomic positions and the ability to model the atoms in a more realistic way, it was expected that more hydrogen atoms could be identified at higher resolution, and that is indeed the case. At 0.95-Å resolution 237 peaks (approximately 100 more peaks than were found at 1.20-Å resolution) were identified as potential hydrogen atoms with 30 peaks previously identified at 1.20-Å resolution. Of the 237 potential hydrogen peaks, 184 peaks are in association with carbon atoms and 53 with nitrogen atoms. Of the 184 peaks associated with carbon atoms, a modest increase in the number of potential C_α hydrogen peaks was observed when increasing the resolution from 1.20 to 0.95 Å, while the number of peaks associated with side chain carbons and amide nitrogen atoms doubled (Table 2). In addition, eight peaks associated with side chain nitrogen atoms were observed at 0.95-Å resolution (none were observed at 1.20-Å resolution). For the 30 identical peaks, 21 were associated with side chain carbons while only five were associated with C_α and four with backbone nitrogen atoms. These numbers are surprisingly low, especially for the main chain carbons and nitrogen atoms, which are typically the most rigidly held atoms in a protein. Several factors may contribute to the low number of identical peaks that may correspond to hydrogen atoms. First, the scattering of a hydrogen atom is weak and falls off more rapidly as resolution and thermal motion increase when compared with heavier atoms. For example, with a temperature factor of 6, the ratio of scattering factors for carbon to hydrogen is approximately 15:1 at 2.0-Å resolution, but drops to approximately 6:1 at 1.0-Å resolution (http://www-structure.llnl.gov/Xray/comp/scatfac.htm). The normal motion of the heavier atoms that associate with hydrogen atoms can reduce the hydrogen contribution to background noise, making it impossible to observe them in a Fourier difference map and difficult to reproduce them from one data set to the next. Aside from normal motion of the protein atoms, a radiation-induced break in the only disulfide bridge of AAP in the 1.20-Å resolution structure may have increased the motion of some side chain and main chain atoms, further reducing the scattering contribution of the associated hydrogen atoms. In the AAP–Tris structure, the overall average B factor is 16 Å^2, while in this structure it is 11 Å^2. Finally, different proton exchange rates for the different pHs used for each structure (8.0 at 1.20-Å resolution and 7.5 at 0.95-Å resolution) may account for the lack of electron density peaks for many of the main chain nitrogen atoms. All of the peaks at 0.95-Å resolution had an electron density level higher than 4.6σ (0.17e^- Å^{-3}) with an average σ level of 6.7 (0.24e^- Å^{-3}) in an electron density map with coefficients $F_{obs}-F_{calc}$.

In the native state, the protonation state of the bridging water species is most likely either H_2O or OH^-. The role of Glu_{151} in the mechanism is dictated by the form of this bridging species [17]. In the H_2O form, a proton must be transferred to Glu_{151} in order to activate the water molecule for attack on the substrate carbonyl. If the bridging species is in the OH^- form, such a transfer is unnecessary and Glu_{151} may accept the proton at a later step of the mechanism, after the C–N bond has already been broken, or it may have some other role in the mechanism. Although the active site is a relatively rigid area of the protein (average *B* value of 7.2 $Å^2$ for all of the active-site residues compared with 10.9 $Å^2$ for the rest of the protein), only four peaks corresponding to hydrogen atoms were located and all of them were associated with carbon atoms. The lack of electron density corresponding to hydrogen atoms is expected for the side chain oxygen atoms of aspartic acid and glutamic acid, and the nitrogen of histidine ligands, since their side chains are within the first and second coordination spheres of the two metal ions and the pH is above the individual pK_as for the liganded amino acid side chains.

The active site at 0.95-Å resolution, pH 7.5

At 0.95-Å resolution the electron density is clearly defined around each atom, even allowing the identity of individual atoms to be determined by their integrated intensity (Fig. 1). Because the positions of all the atoms were not restrained during refinement, precise Zn–ligand and C–O distances could be obtained without bias. The average Zn–N distance in the first coordination sphere of both metal ions is 2.03 Å and the average Zn–O distance is 2.07 Å, while in the second coordination sphere the average Zn–O distance is 2.39 Å (Table 3). A superposition of all atoms in the active sites of the 0.95-Å resolution structure and the 1.20-Å resolution structure overlaid with an rms deviation of 0.07 Å. The structure solved to 1.20-Å resolution showed a molecule of Tris from the buffer solution coordinated to both metal ions via four contacts [8]. In the native enzyme crystallized in HEPES, the Fourier difference electron density map with coefficients $2F_{obs}–F_{calc}$ and $F_{obs}–F_{calc}$ showed one well-formed sphere of electron density positioned between both metal ions that remained visible up to 9.5σ level in the Fourier difference map with coefficients $2F_{obs}–F_{calc}$, a σ level that is consistent with other oxygen atoms located in the active site (Fig. 1). A model oxygen atom was placed into the sphere of electron density and included in further refinement, resulting in an improvement in the electron density. This oxygen corresponds to the metal-bridging solvent-derived oxygen species.

Table 3. Zn–X distances (Å) of active-site metal ligands at 0.95-Å resolution

Amino acid	Ligand	Zn_1^{2+}	Zn_2^{2+}	C–O distance (Å)
His_{97}	NE2		2.03 (0.01)	
Asp_{117}	OD1		2.00 (0.05)	1.26 (0.01)
	OD2	2.04 (0.06)		1.28 (0.01)
Glu_{152}	OE2	2.13 (0.01)		1.28 (0.01)
	OE1	2.48 (0.01)		1.25 (0.01)
Asp_{179}	OD1		2.11 (0.01)	1.21 (0.01)
	OD2		2.31 (0.01)	1.25 (0.01)
His_{256}	NE2	2.03 (0.01)		
OH^-	O	2.01 (0.01)	1.93 (0.01)	
Zn_1			3.33 (NA)	

The calculated estimated standard deviation associated with each distance is shown in *parentheses*

Electron density corresponding to potential hydrogen atoms in the active site was not observed in the Fourier difference map with coefficients $F_{obs}–F_{calc}$; however, the protonation state of the bridging oxygen species can be determined by comparing Zn–O distance standards found in the CSD [9] and those studied by computational methods [10] with the precise Zn–O distances obtained in this structure. These standard values indicate that the average Zn–OH coordination distance is approximately 1.90–2.00 Å, while the average Zn–OH_2 coordination

distance is 2.10–2.20 Å. The Zn–O distances for the bridging oxygen species in this structure are 2.01 Å to Zn_1 and 1.93 Å to Zn_2, suggesting the bridging oxygen species is an OH^-. Furthermore, the projection of the anisotropic displacement parameter of the bridging oxygen atom points in the direction of a carboxylate oxygen of Glu_{151}, suggesting that Glu_{151} is indeed responsible for accepting a proton from the bridging water molecule as it becomes activated to OH^- [17].

The distribution of the double bond of the zinc liganded carboxylates can have three possible configurations [8]. Since real standard deviations in the bonding distances were calculated (Table 3, in parentheses), a comparison of the active-site carboxylate carbon–oxygen distances with those found in small molecules may enable us to distinguish between the three configurations. For small molecules, the average C–O bond distance for a carboxylate is 1.26–1.28 Å while that for C=O of the corresponding acid is 1.22 Å [18]. In AAP, the carbon–oxygen distances of the two side chain carboxylate oxygen atoms of Asp_{117}, the bridging protein ligand, are equal with respect to each other and are consistent with distances found in small molecules for C–O (Table 3). This implies the electron distribution of the double bond is equal between the two carbon–oxygen bonds (Fig. 2), as might be expected for a carboxylate whose side chain oxygen atoms are both used as inner-sphere metal ligands. For Glu_{152}, the carbon–oxygen distances are also equal with respect to each other, within the associated limits of the error; however, when compared with the other active-site carboxylates, they are longer than the carbon–oxygen distances of Asp_{179} and similar to those of Asp_{117}, suggesting the double bond is evenly distributed between the two oxygen atoms and that the carboxylate is fully ionized. The oxygen of Glu_{152} that is not in the first coordination sphere of the Zn ion, referred to as the dangling oxygen, is positioned 3.15 Å from the bridging water species and 3.20 Å from a side chain oxygen of Glu_{151}. If the bridging oxygen species is OH^- and Glu_{151} is the proton acceptor [17], then the dangling oxygen of Glu_{152} may serve to stabilize the bridging hydroxide ion or the protonated carboxylate side chain by forming a hydrogen-bonding interaction with them.

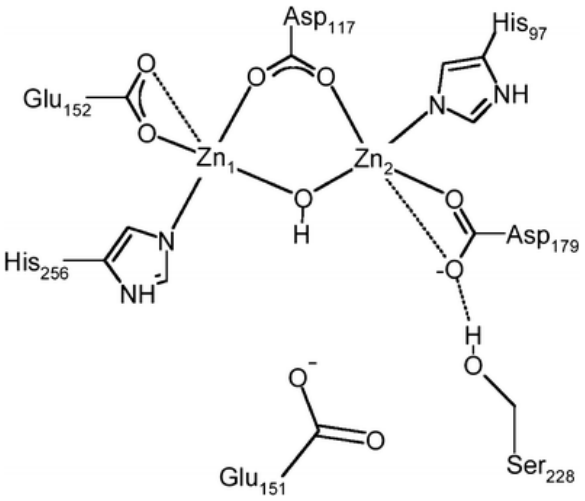

Fig. 2. Schematic of the active site of native aminopeptidase from *Aeromonas proteolytica* (*AAP*)

For Asp_{179}, there is a 0.04-Å difference in bond length between the two carbon–oxygen bonds of the side chain carboxylate, with the distance to the inner-sphere oxygen being slightly shorter than the dangling oxygen distance. This difference is about twice the ESD of the distance measurement at this resolution. Although a comparison of these two bond distances with each other may be unreliable because the difference between them is near the limits of their error estimates, a comparison can be made between the carbon–oxygen distances of Asp_{179} and those of Asp_{117} and Glu_{152}. The carbon–oxygen distance to the inner-sphere oxygen of Asp_{179} is significantly shorter than the carbon–oxygen distances for the metal ligated oxygen atoms of Glu_{152} and Asp_{117} (Δd=0.05–0.07 Å) and is consistent with that for C=O distances measured in small molecules, implying that this bond has more double-bond character. The carbon–oxygen distance for the dangling oxygen compares well

with the C–O distances for Glu_{152} and Asp_{117} and is consistent with the C–O distance of small molecules, suggesting that this bond has more single-bond character. The apparent localization of the double bond to the inner-sphere oxygen is unusual; however, it is likely facilitated by a hydrogen-bonding interaction between the dangling oxygen with the side chain oxygen of Ser_{228} and a water molecule that also shares a hydrogen with the carbonyl oxygen of Cys_{227}. Additionally, potential hydrogen-bonding interactions of the N_{δ} proton of His_{97} with a side chain oxygen of Asp_{99} forming an Asp–His–Zn triad that has been postulated to decrease the Lewis acidity of Zn(II) ions [19] and may further assist in facilitating the coordination of a double-bonded oxygen to Zn_2.

Active site at 1.24-Å resolution, pH 4.7

One of the first steps in the proposed reaction mechanism is the coordination of the substrate's carbonyl oxygen of the N-terminal amino acid to Zn_1. Upon substrate binding, the coordination geometry of Zn_1 changes from four coordinate to five coordinate, resulting in a weakening of the Zn_2–O interaction and a longer Zn_2–O distance is observable at high resolution. If the bridging oxygen in the native enzyme is an OH^-, as identified earlier herein, then the level of precision obtained at high resolution should make it possible to observe the 0.1–0.2-Å change that should occur in Zn–O distances when the bridging oxygen changes its protonation state from OH^- to OH_2.

The 1.24-Å resolution crystal structure of AAP was solved at pH 4.7, a pH at which the bridging oxygen is expected to contain two protons [20]. At this resolution, ESDs of the individual bonding distances cannot be obtained because of the low data-to-parameter ratio. However, the average rms deviation from ideality is 0.02 Å. At pH 4.7, the Zn_1–O distance is 2.19 Å, an increase of 0.19 Å over its value at high pH, and the Zn_2–O distance remains the same when compared with the Zn–O distances at pH 7.5 (Fig. 3). Zn_1 has gained an additional ligand at low pH and become five coordinate; the coordination number for Zn_2 remains unchanged at 4. The increase in the Zn_1–O coordination distance may be the result of adding a proton to the bridging hydroxide ion, the change in the coordination number of Zn_1 from 4 to 5, or both. A coordination number change is the most likely cause since the Zn_2–O distance remains consistent with that observed for Zn–OH, suggesting that the bridging solvent species has not taken on a second proton. The change in Zn_1 coordination geometry is the result of a second molecule of water that coordinates within the first coordination sphere of Zn_1, increasing its coordination number; however, a comparison of the carbon–oxygen distances at this resolution was not possible.

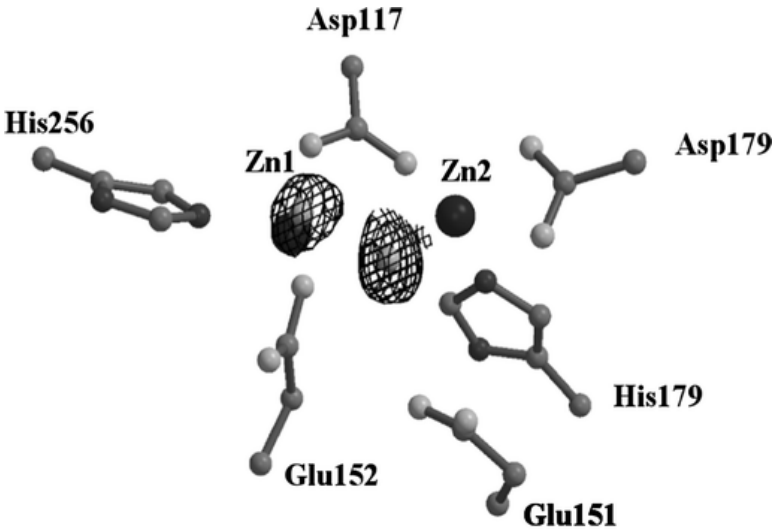

Fig. 3. The active site for AAP at pH 4.5. A $2F_o–F_c$ electron density map corresponding to the bridging oxygen atom and a second water species coordinated to Zn_1 contoured at 1.7σ. The rest of the active-site density has been removed for clarity

This low pH structure may serve as a simple model for the first step in the proposed chemical reaction mechanism of AAP, which proposes the coordination of the carbonyl oxygen of the N-terminal amino acid to Zn_1, increasing the coordination number of Zn_1 from 4 to 5, thereby weakening the Zn_1–OH–Zn_2 bridge. This is exactly what is observed in the X-ray crystallographic data in that the Zn_1–OH bond distance increases to 2.19 Å, a reasonable bonding distance, but clearly a weakened bond from the pH 7.5 X-ray structure. These data are exactly what one would predict based on chemical principles since the addition of an electron pair from H_2O to Zn_1, which would be a better σ donor than a carbonyl group, makes Zn_1 more electron rich. Therefore, lengthening of the Zn_1–OH bridging oxygen distance allows the Zn_1 center to maintain charge neutrality. A result of the increase in the Zn_1–OH bond distance is the strong Zn_2–OH interaction (1.93 Å). This short Zn_2–OH distance is consistent with the observed decrease in single-bond character of the Zn_2–O carboxylate oxygen atom interaction, since the added electron density of the bridging OH^- group to Zn_2 forces the Zn_2 center to displace some negative charge in order to maintain charge neutrality.

Movement of metal ions during catalysis

During the course of the enzymatic reaction, the distances of the metal ions to their ligands may change in accordance with the chemical state of the substrate/intermediate. The metal ions must be able to move in response to a constantly changing local environment in order to accommodate these changes. Such movements have been observed in many other bridged binuclear metalloenzymes and it is possible that they are a common feature in all of them. At 1.8-Å resolution, the resolution at which several crystal structures of AAP have been studied, it is impossible to assess the thermal motion of the atoms because of the isotropic treatment of the thermal parameters. The active site of AAP appeared to be symmetric with respect to metal ion coordination and thermal motion. The ability to refine anisotropic displacement parameters at 0.95-Å resolution, however, allows for an opportunity to quantitate the thermal motion of the active-site atoms. The anisotropic treatment of thermal motion has indicated that the active site is actually asymmetric with one metal binding site being more rigid than the other. The average B_{iso} value for all of the active-site amino acids is 7.17 $Å^2$ compared with 10.85 $Å^2$ for all protein atoms, indicating the active-site amino acids are slightly more rigid with respect to the rest of the enzyme. The side chain residues liganded to Zn_1 have an average B_{iso} value of 8.47 $Å^2$, which is significantly higher than the average B_{iso} value for the ligands to Zn_2 (7.01 $Å^2$). This relative increase in the thermal motion of the Zn_1 nonbridging ligands can be attributed to the lack of possible protein hydrogen-bonding partners for Glu_{152} and His_{256}. On the other hand, the nonbridging ligands to Zn_2 have potential protein hydrogen-bonding partners. The dangling oxygen of Asp_{179} is in position to share a hydrogen with the side chain oxygen of Ser_{228}, while His_{97} likely shares a hydrogen with a side chain oxygen or the carbonyl oxygen of Asp_{99}. These potential hydrogen-bonding partners may serve to stabilize the Zn_2 binding pocket. As a consequence of the thermal motion of the Zn_1 side chain ligands, Zn_1 (B_{iso}=6.98 $Å^2$) has more thermal motion than Zn_2 (B_{iso}=5.55 $Å^2$).

The Zn_1 binding site was also shown to be more flexible than the Zn_2 site when a transition-state analog inhibitor binds to the enzyme. l-Leucinephosphonic acid (LPA) interacts with AAP to form a complex whose structure is expected to resemble the transition state in the hydrolysis reaction catalyzed by AAP [6]. When the active-site amino acids and metal ions of the AAP–LPA complex are superimposed onto the same atoms in the native enzyme (rms 0.206 Å) the Zn–Zn distance increases from 3.33 to 3.9 Å in the LPA-bound form (Fig. 4). LPA coordinates to both zinc ions and pushes Zn_1 0.60 Å away from its position in the native enzyme, while Zn_2 remains close to its original position. These data are also consistent with the idea that Zn_1 can move during the catalytic reaction in order to accommodate the binding of substrate or the stabilization of the transition state. To make way for the Zn_1 movement, His_{256} shifts away from the center of the active site by 0.06 Å and rotates 2° around the C_α–C_β bond. The residues around Zn_2 do not undergo any conformational changes, consistent with a more rigidly bound metal ion.

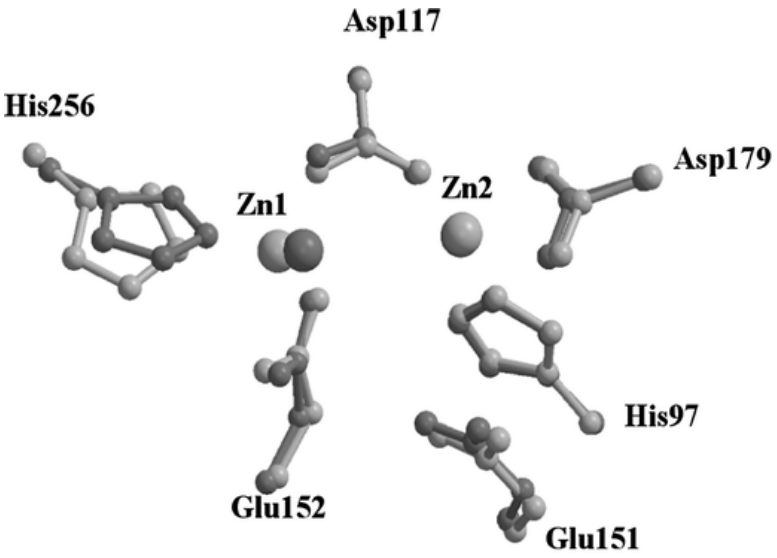

Fig. 4. A superposition of the active-site atoms of AAP with the active-site atoms of the AAP–l-leucinephosphonic acid (*LPA*) complex. The atoms in *dark gray* represent the active site for the native enzyme, while those in *light gray* represent the AAP–LPA complex. LPA has been stripped away for clarity

Insight into the chemical mechanism

The structures of AAP presented herein have provided additional evidence for the proposed reaction mechanism of AAP that was not obtainable from lower-resolution X-ray structures. In the native enzyme, the bridging oxygen species has been identified as OH^-, indicating that the metal ions activate the bridging solvent molecule before substrate binding (Fig. 5, species 1). Glu_{151}, the proton acceptor in this activation step [17], donates a proton to the penultimate nitrogen of the product later in the reaction cycle. On the basis of kinetics, spectroscopic and X-ray crystallographic data [6, 21] it has been proposed that substrate coordinates to the bimetallic center in a stepwise fashion with the carbonyl oxygen of the N-terminal amino acid first coordinating to Zn_1 followed by the coordination of the free amine to Zn_2 (Fig. 5, species 2 and 3). Spectroscopic evidence for Co(II)-substituted AAP indicates that the two metal ions in the AAP active site bind in a sequential fashion and that upon introduction of substrate the coordination geometry of the first metal binding site changes from four to five coordinate. In addition, the bridging solvent molecule becomes terminal and is bound to the first metal binding site. This terminal solvent molecule is then proposed to attack the activated carbonyl carbon of the substrate, forming a four-membered ring and a tetrahedral substrate intermediate (Fig. 5, species 4). The attacking oxygen, coordinated to Zn_1, migrates to Zn_2 through an interaction with Glu_{151} to give species 5 in Fig. 5.

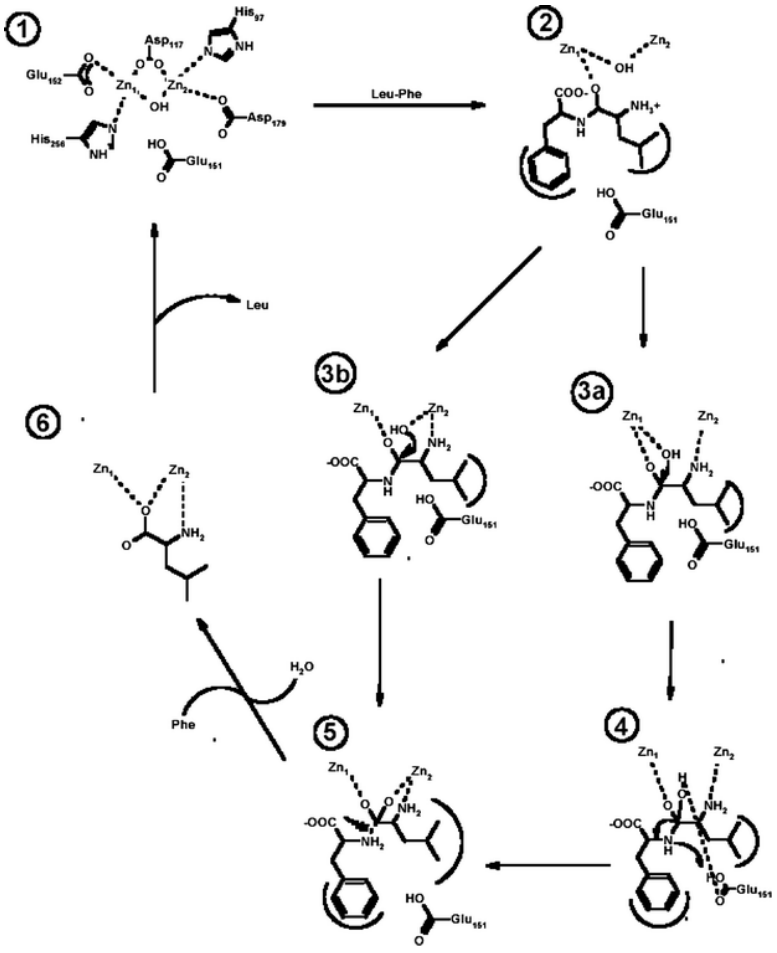

Fig. 5. Proposed chemical reaction mechanisms for AAP

On the basis of X-ray crystallographic and spectroscopic studies of AAP complexed with the substrate analog inhibitor 1-butaneboronic acid (BuBA) [21], the metal ion thought to play the catalytic role was identified as Zn_1. The X-ray crystal structure shows that BuBA binds to the bimetallic center by coordinating two of its oxygen atoms to Zn_1 with Zn–O distances of 2.7 and 2.5 Å and positions its *n*-butyl tail into the hydrophobic pocket near the active site. A molecule of water was also observed near the active site. BuBA is a slow-binding competitive inhibitor of AAP and the X-ray crystal structure has been proposed to represent an arrested form of the reaction between the Michaelis complex and the transition state [21]. Since AAP is 80% active with only one metal ion present and BuBA only forms contacts to Zn_1, it was proposed that Zn_1 is the metal ion required for catalysis. The coordination of BuBA may represent an intermediate in the reaction pathway; however, the Zn–O distances are quite long and, for AAP, are typical distances for atoms that do not directly bind to the metal ions. On the basis of structural studies of the native enzyme and intermediates that mimic putative reaction intermediates, the Zn–O distances are expected to be approximately 0.4–0.6 Å shorter than those reported for BuBA. In addition, the mechanism proposes that the bridging hydroxide ion becomes terminal to one of the metal ions before attacking the activated substrate. If the water/hydroxide is bound to one of the Zn(II) ions, the Zn–OH distance to that metal ion would be expected to be approximately 1.9–2.0 Å, but in the BuBA structure, the water molecule that was proposed to be the attacking nucleophile resides over 4.0 Å from either zinc ion, indicating that it is not a ligand to either metal ion. Therefore, the BuBA structure may better represent a catalytic step where the nucleophile has been delivered, the C–N bond has been broken, and the product is being released from the enzyme active site.

The 1.24-Å resolution structure of AAP at pH 4.5 revealed a change in the coordination number of Zn_1 from four to five coordinate accompanied by a weakening in the Zn_1–OH bond. The Zn_2–OH bond distance remained the same, suggesting that upon the change in coordination number of Zn_1, the bridging hydroxide ion shifts electron density to Zn_2. Although one cannot be sure that the structure of AAP at a pH approximately four units below the optimum pH for enzymatic activity reflects the correct Zn(II) geometry of a productive step in the catalytic pathway, it may provide information about the differences in the behavior of the two metal ions in the nearly symmetrical AAP active site. If this structure serves as a model for the initial substrate binding step in the chemical reaction pathway of AAP, two intermediate species (Fig. 5, species 3a or 3b) can be proposed. For intermediate 3a to form, the second substrate binding step would involve coordination of the N-terminal amine to Zn_2 followed by breaking of the Zn_2–OH bond, consistent with spectroscopic and X-ray crystallographic data. However, the N-terminal amine binding step to Zn_2 is unaccounted for in the pH 4.5 structure. Alternatively, N-terminal amine binding to Zn_2 does not facilitate the loss of a Zn_2–OH bond resulting in a Zn_2-associated hydroxide ion attacking the activated carbonyl carbon of the substrate. This reaction pathway leads to the direct formation of a stable five-membered ring for the tetrahedral intermediate (Fig. 5, species 5). The role of Zn_1 would then be to assist in stabilizing the bridging hydroxide ion in the native enzyme and in activating the carbonyl carbon of the N-terminal amino acid.

Intermediate 3b differs from the intermediate previously proposed in that it reverses the roles proposed for each metal ion in catalysis. Distinguishing the contributions of the two identical Zn(II) ions in AAP is an important question since AAP displays 80% of its total activity level with only a single metal ion bound. Therefore, the two Zn(II) ions play separable roles in catalysis. With each new structure of AAP, we gain additional information about the catalytic roles of each of these metal ions, allowing us to refine our proposal for their function. Discriminating between the functions of Zn(II) ions on the basis of the binding of inhibitors, whose interactions with the two Zn(II) ions may be dominated by their metal-chelating properties rather than by any resemblance to the way a substrate binds or the structures of unbound enzyme at extremes of pH, is at best an uncertain proposition. Definitive assignment of the roles of each of the Zn(II) ions awaits a high-resolution structure of a productive enzyme–substrate complex, a difficult but worthwhile goal for this class of enzyme.

Notes

Acknowledgements

This work was supported by the National Science Foundation (CHE-0549221 to R.C.H.), by the National Institutes of Health (GM26788 to G.A.P. and D.R.), and, in part, by the Macromolecular Training Grant from the National Institutes of Health (W.D.).

References

1. Sträter N, Lipscomb WN, Klabunde T, Krebs B (1996) Angew Chem Int Ed Engl 35:2024
2. Wilcox D (1996) Binuclear metallohydrolases. Chem Rev 96:2435–2458
3. Lipscomb W, Sträter N (1996) Chem Rev 96:2375–2434
4. Dismukes G (1996) Chem Rev 96:2909–2926
5. Prescott J, Wilkes S (1976) Methods Enzymol 45:530–543
6. Stamper C, Bennett B, Edwards T, Holz R, Ringe D, Petsko G (2001) Biochemistry 40:7035–7046Bzymek KP, Holz RC (2004) J Biol Chem 279:31018–31025
7. Desmarais WT, Bienvenue DL, Bzymek KP, Holz RC, Petsko GA, Ringe D (2002) Structure 8:1063–1072
8. Harding MM (1999) Acta Crystallogr D 55:1432–1443
9. Diaz N, Suarez D, Merz KM Jr (2000) J Am Chem Soc 122:4197–4208
10. Schalk C, Remy J, Chevrier B, Moras D, Tarnus C (1992) Arch Biochem Biophys 294:91–97
11. Chevrier B, Schalk C, D'Orchymont H, Rondeau J-M, Moras D, Tarnus C (1994) Structure 2:283–291
12. Otwinowski Z, Minor W (1997) Methods Enzymol 276:307–326

13. Brunger AT, Adams PD, Clore GM, Delano WL, Gros P, Grosse-Kunstleve RW, Jiang J-S, Kuszewski J, Nilges M, Pannu NS, Read RJ, Rice LM, Simonson T, Warren GL (1998) Acta Crystallogr D 54:905–921
14. Sheldrick G, Schneider T (1997) Methods Enzymol 277:319–343
15. Lamzin VS, Wilson KS (1993) Acta Crystallogr D 49:129–147
16. Holz RC (2002) Coord Chem Rev 232:5–26
17. Barrow GM (1981) Physical chemistry for the life sciences, 2nd edn. McGraw-Hill, New York, p 432
18. Christianson DW, Alexander SA (1989) J Am Chem Soc 111:6412–6419
19. Baker JO, Prescott JM (1983) Biochemistry 22:5322–5331
20. De Paola CC, Bennett B, Holz RC, Ringe D, Petsko GA (1999) Biochemistry 38:9048–9053